Models of the δ Scuti Variable AN Lyn as a Multiple Star System

Scott Curtis

A senior thesis submitted to the faculty of
Brigham Young University
in partial fulfillment of the requirements for the degree of

Bachelor of Science

Dr. Eric Hintz, Associate Chair

Department of Physics and Astronomy

Brigham Young University

ABSTRACT

Models of the δ Scuti Variable AN Lyn as a Multiple Star System

Scott Curtis
Department of Physics and Astronomy, BYU
Bachelor of Science

AN Lyncis (AN Lyn) is a δ Scuti variable which has been observed and analyzed since 1981. Three independent periods have been identified in AN Lyn, though one frequency, 9.5598 c/d, has never been confirmed outside of its original publication. Recent studies have attempted to explain AN Lyn's complicated $O-C$ behavior through constant period changes or potential companions. However, models have struggled to describe all the data. In this work, we analyze new data taken at the Orson Pratt Observatory and from NASA's TESS. We derive a new primary pulsation frequency, $f_1 = 10.17555(5)$, find $f_3 = 9.4091$ which resembles the previously unconfirmed frequency, and explain AN Lyn's $O-C$ diagram using various models of the light travel time effect. We find that AN Lyn is well-described as a three-body system. We use various models and a Monte Carlo simulation to constrain stellar and orbital parameters. We find that its inner and outer companions have $M \sin i$ of $0.1535 M_{\odot}$ and $0.4896 M_{\odot}$, respectively. These results will help us understand this complicated system and identify it as an intriguing target for observation in the future.

Keywords: δ Scuti Variable, Light-time Effect, Triple System, O–C Diagram

ACKNOWLEDGMENTS

I would like to thank my thesis advisor, Dr. Eric Hintz, for his support in research and writing. I would further like to thank the faculty and students running the Orson Pratt Observatory for taking much of the data used in this analysis. This research has made use of the SIMBAD database, operated at CDS, Strasbourg, France. This paper includes data collected by the TESS mission, which are publicly available from the Mikulski Archive for Space Telescopes (MAST). Funding for the TESS mission is provided by NASA's Science Mission directorate. This work was supported in part by undergraduate research funding through experiential learning grants from the College of Computational, Mathematical, and Physical Sciences at Brigham Young University.

Contents

List of Figures

List of Tables

Chapter 1

Introduction

Pulsating variable stars vary in brightness over time, often in a regular pattern. They range from short-period variables with periods of minutes to long-period variables with periods of years (Percy 2007). The pattern of brightening and dimming is caused by the expansion and contraction of the star's outer layers. Several mechanisms can be responsible for this behavior, including the opacity-driven κ mechanism. Under the κ mechanism, as a partially ionized layer of a star contracts due to gravity, it becomes more dense and opaque, trapping radiation and heat (Zhevakin 1963). This increase in temperature leads to thermal expansion, cooling the star (Carroll & Ostlie 2017). The cooler star then contracts under gravity repeating the process.

δ Scuti stars are variable pulsator stars of spectral type A to F located in the instability strip of the H-R diagram (Breger 1979). They have typical periods on the order of 0.25 days and a pulsation amplitude, or difference in brightness between maximum and minimum, of several mmag to roughly 0.8 mag (Carroll & Ostlie 2017). δ Scuti stars pulsate in both spherically-symmetric radial and non-radial modes (Handler 2009). The κ mechanism drives their pulsation. δ Scuti stars are of particular interest in the field of asteroseismology which uses pulsation modes to probe the inner layers of stars (Percy 2007). Data from δ Scuti and other pulsating stars enable us to refine stellar models and understand what is going on beneath a star's surface (Handler 2009).

In order to study these stars, we use a variety of tools including observed minus calculated ($O-C$) diagrams obtained from photometric observations and radial velocities derived from spectrographic observations. After the photometric images are reduced, we analyze and plot the brightness of the star over time in what is called a light curve. Then, to establish the primary pulsation period/frequency, we identify the precise times that the star reached the brightest point of a pulsation cycle. These points in time are called maxima. The time interval between two consecutive maxima is the primary pulsation period. Once several maxima have been determined, we assign one as the maximum of cycle zero and then assign cycle numbers sequentially. Unless we continuously observe a star, there are gaps in our data (due to daytime, bad weather, etc.). In order to determine how many cycles pass between observations, we take the difference in Heliocentric Julian Date (HJD) divided by the period. This information can be summarized into an equation called the ephemeris (Percy 2007). A linear ephemeris is of the form

$$HJD_{max}(E) = E_0 + E \times P, \tag{1.1}$$

where $HJD_{max}(E)$ is the time of maximum light for the E^{th} cycle, E_0 is the HJD of the first maximum, and P is the primary pulsation period.

With this information, we can perform Fourier frequency analysis to identify other, less obvious, frequencies. We can also construct an $O-C$ diagram which plots the difference between when we observe the maxima to occur and when we expect them to occur based on the primary frequency and cycle number. $O-C$ diagrams can reveal other information, such as an evolutionary change in period or the existence of companion stars (Sterken 2005). Radial velocities obtained from spectroscopic data can yield similar information.

This work analyzes the star AN Lyncis (AN Lyn, $\alpha_{2000} = 09^h14^m28.69^s$, $dec_{2000} = +42°46'38.36"$, $V = 10.64$), a multi-periodic, medium-amplitude δ Scuti star 720 $\pm$ 160 pc away (Li et al. 2018; Zhou et al. 2017). AN Lyn was first identified as a variable star by Yamasaki et al. (1981). They reported a primary period of 0.0982747 days and identified it as a δ Scuti star. Agerer et al. (1983)

independently discovered AN Lyn two years later, also identifying it as a δ Scuti star. Since then, AN Lyn has been the subject of numerous studies. Rodriguez et al. (1997a) identified three independent frequencies within the pulsation ($\nu_1 = 10.1756$, $\nu_2 = 18.1309$, and $\nu_3 = 9.5598$ c/d). (Note that frequencies found in the literature are denoted by ν while frequencies found in this work are denoted by f.) Although ν_3 was not subsequently confirmed, the first two frequencies were (although Li et al. (2018) argued that 18.1309 c/d is instead the linear combination of frequencies 28.311 $c/d - 10.1721$ c/d). $O-C$ analysis of AN Lyn revealed that it may be a binary system with an orbit of 26-30 years (Hintz et al. 2005; Zhou et al. 2017). After further analysis, Li et al. (2018) raised the possibility that AN Lyn might be a 3-body system with minimum companion masses 0.51 $\pm$ 0.08 $M_\odot$ and 0.4 $\pm$ 0.1 $M_\odot$ and orbital periods of 66 $\pm$ 5 yr and 24 $\pm$ 2 yr.

In this work, we improve models of AN Lyn as a 3-body system by analyzing the $O-C$ diagram built from photometric and spectral observations. Our $O-C$ diagram improves on earlier publications in two important ways: including more maxima and using a more precise fundamental pulsation period. In Chapter 2, we describe photometric and spectroscopic observations and data reduction, present 319 new maxima—including those obtained from the Transiting Exoplanet Survey Satellite (TESS; Ricker et al. (2014)), and derive a new ephemeris. In Chapter 3, we discuss short-term periods in the light curve and long-term periods in the $O-C$ diagram. We also introduce models of AN Lyn as a 3-body system. Finally, in Chapter 4, we analyze the models, derive lower-bound masses of companion stars, and discuss future work.

Chapter 2

Methods

Because we cannot directly experiment with stars, we use a variety of methods to study them. Since δ Scuti stars change brightness in time, it makes sense to track those changes and learn from them. To do this, we use time-series photometry, the method of determining how bright an object is over time. In δ Scuti stars, it requires many images over the course of 1–2 hours. Thus, most of our data come from these observations. Another important tool for studying stars are spectra, which we also use in our analysis.

2.1 Photometric Data

We took new observations on 45 nights from 2024 to 2025 at the Brigham Young University (BYU) Orson Pratt Observatory (OPO) on 6 inch, 8 inch, and 12 inch telescopes and collected 5 nights of observations from 2015 at the BYU West Mountain Observatory (WMO). We also collected photometric data of AN Lyn published by Rodriguez et al. (1997a;b). Their observations of AN Lyn were carried out at the Sierra Nevada Observatory in Spain (0.9 m telescope) and the San Pedro Martir observatory in Mexico (1.5 m telescope) on a total of 30 nights between February 1994 and May 1996. Their observations were obtained in the Strömgren–Crawford $uvby\beta$ system, and we used the *v*-band data to determine times of maximum light. Our analysis of these data yielded negligible differences to those published by Rodriguez et al. (1997a) and Zhou (2002). Finally, we used light curves taken from TESS in the Peranso 3.1 software (Paunzen & Vanmunster 2016).

We reduced the BYU data using IRAF with the standard bias, dark, and flat corrections, then obtained light curves in AstroImageJ (Collins et al. 2017). We used the comparison stars TYC 2990-19-1, GSC 02990-00001, TYC 2990-221-1, and TYC 2990-575-1 (see table 2.1 and figure 2.1). BYU, TESS, and Rodriguez light curves were analyzed in Peranso after applying a heliocentric correction to ensure the times were in HJD. We fit 4- or 5-degree polynomials to the light curves around the maxima and found the local maximum to determine precise times of maximum light.

We obtained 63 maxima from the OPO and 9 maxima from the WMO. 17 maxima were in the R filter and the remaining 46 were in the V filter. We also obtained 35 maxima from the Rodriguez et al. data and 247 maxima from TESS. Due to the rich observation history of AN Lyn, we were also able to collect 632 previously published maxima (Li et al. 2018; Zhou et al. 2017). Utilizing this large amount of data, we can study AN Lyn's behavior with greater accuracy than previously possible.

Table 2.1 Check Stars Used for Photometry. V magnitudes are from the American Association of Variable Star Observers (AAVSO) Photometric All-Sky Survey (APASS).

Check Number	Star Identifier	RA (J2000)	Dec (J2000)	*V*
C1	TYC 2990-19-1	09:14:34.72	+42:41:02.0	10.973
C2	GSC 02990-00001	09:14:36.62	+42:48:23.8	12.322
C3	TYC 2990-221-1	09:14:53.35	+42:51:12.1	12.053
C4	TYC 2990-575-1	09:14:01.15	+42:55:22.8	11.583

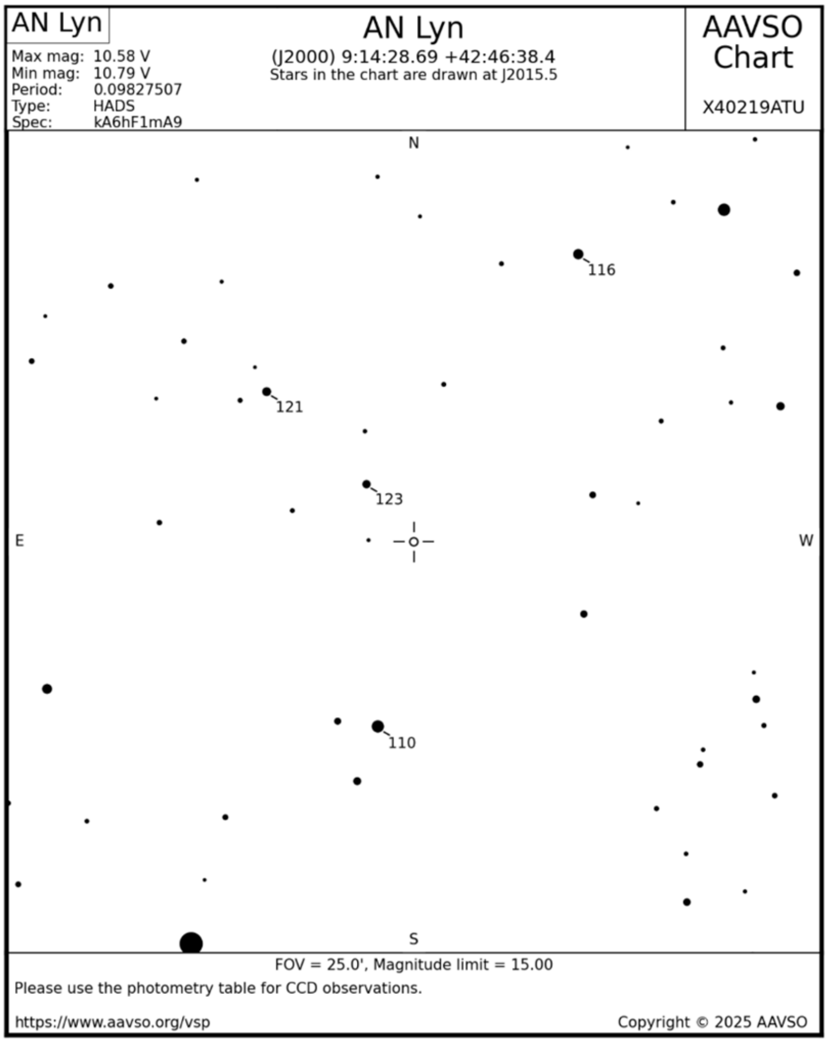

Figure 2.1 A finder chart taken from the AAVSO variable star plotter. AN Lyn is located at the cross hairs in the center of the image while comparison stars C_1, C_2, C_3, and C_4 are labeled 110, 123, 121, and 116 respectively.

2.2 Spectral Data

In addition to photometric observations, spectral data yield insights into pulsations and stellar motion. By identifying the deviation of spectral lines in AN Lyn's spectrum from their rest wavelength, we can calculate Doppler shift. From the Doppler shift, we calculate a radial velocity (RV) which encodes the pulsation of the star's outer layers as well as the star's motion with respect to the observer. Using the known primary pulsation period, we can separate these effects.

Between 2011–2021, we obtained 59 spectra at the Dominion Astrophysical Observatory (DAO). Spectra were reduced using standard procedures in IRAF. To determine radial velocities (RV), we analyzed the redshift of the hydrogen (H) H-alpha (6562.80 Å) and H-beta (4861.33 Å) lines, as well as the sodium (Na) doublet (5889.95 Å, 5895.92 Å) in our spectra using the RVIDLINES package within IRAF. We also collected 12 RVs from 2004 from Hintz et al. (2005).

2.3 Ephemeris

In order to create an accurate $O-C$ diagram, one needs to know the pulsation period precisely. Any deviation from the true period becomes magnified as we analyze data spanning tens of thousands of pulsation cycles. The period is determined by averaging the time between many sets of consecutive maxima. This period can then be used to create an equation—the ephemeris—which predicts when the maxima will occur. To determine the primary pulsation period, we utilized TESS data.

One advantage of TESS data is its continuity. The light curve from TESS is made up of over 18,000 data points spanning 28 days from Jan 22, 2020 to Feb 18, 2020. Other than a gap from the night of Feb 2 to the morning of Feb 7, exposures were taken every two minutes resulting in a continuous, high-precision light curve. This makes TESS data ideal for creating an ephemeris as well as detecting short-term frequencies. In order to define a new ephemeris, we plotted TESS maxima times against cycle number beginning at 0 and extending to 276 and calculated a best-fit line:

$$HJD_{max} = 2458870.57037(7) + 0.0982747459(4913)E.$$

From our linear best-fit, we define a new fundamental pulsation period: $P_1 = 0.09827475(49)$ days and the corresponding frequency: $f_1 = 10.17555(5)$. In order to maintain ease of comparability, we adopted the initial epoch from Zhou et al. (2017) to form our final ephemeris:

$$HJD_{max} = 2452307.077419 + 0.0982747459(4913)E. \tag{2.1}$$

2.4 Period Analysis

As a δ Scuti variable, AN Lyn's pulsations are visible through a Fourier analysis of the photometric data. Yamasaki et al. (1981) first identified $\nu_1 = 10.1756$ c/d, and determined AN Lyn was monoperiodic. Rodriguez et al. (1997b) similarly identified ν_1, but also identified two more independent periods: $f_2 = 18.1309$ c/d, and $\nu_3 = 9.5598$ c/d. Zhou (2002), Hintz et al. (2005), Zhou et al. (2017), and Li et al. (2018) each confirmed ν_1, ν_2, and interactions (such as $\nu_1 + \nu_2$) but did not find ν_3.

We conducted a period analysis of AN Lyn's pulsations using TESS data. In addition to its high number of exposures, TESS data are unaffected by atmospheric effects or differences in filter, detector, or telescope optics. These advantages lead to the most detailed light curve of AN Lyn to date, making it ideal for period analysis.

Chapter 3

Results

Short- and long-term periods can be used to analyze AN Lyn's behavior. We performed a frequency analysis of the TESS data to search for short-term periods and constructed an $O-C$ diagram to search for long-term periods. This diagram is the main focus of our analysis and bridges the gap between time-series photometry and the physical properties of AN Lyn.

3.1 Short-term Periods

Because the data from TESS are mostly continuous, we prioritized these data in our frequency analysis. We performed a Fourier analysis in Peranso (Paunzen & Vanmunster 2016), and found three independent frequencies: f_1, f_2, and f_3 (see figure 3.1). Table 3.1 lists the frequencies we found in order of highest relative power.

Of particular interest is f_3 as it resembles the period ν_3 found in Rodriguez et al. (1997a). ν_3 has not been confirmed by subsequent studies. Our f_3 differs from ν_3 by approximately 0.1507 cycles per day. It is interesting to note that f_3 appears in the Fourier analysis of both the TESS observational data and the TESS $O-C$ data (see figure 3.2). However, f_3 only appears noticeably after prewhitening f_1 in the former (see figures 3.1e and 3.1f), and in the latter, it appears to be a

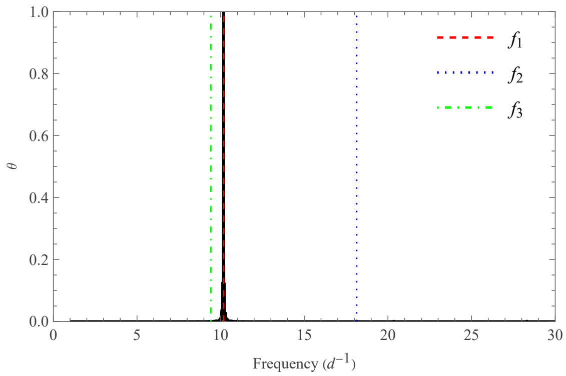

(a) The normalized periodogram of TESS observations of AN Lyn. f_1, f_2, and f_3 are denoted with vertical lines.

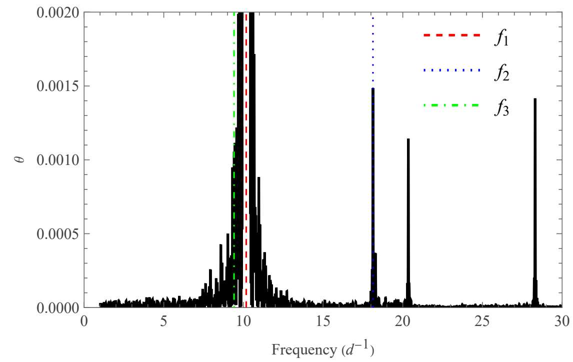

(b) A zoomed-in view of the periodogram. $2f_1$ and $f_1 + f_2$ are also visible at 20.3510 and 28.3072 and respectively.

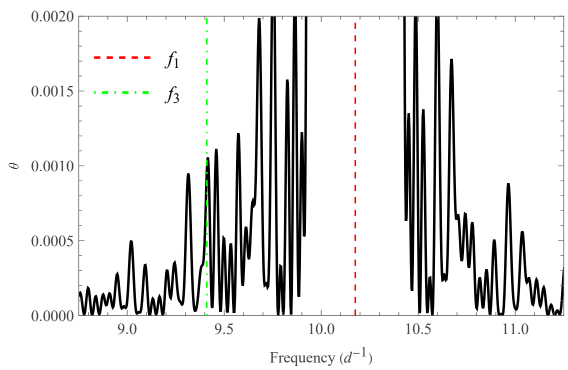

(c) The periodogram zoomed-in on f_3.

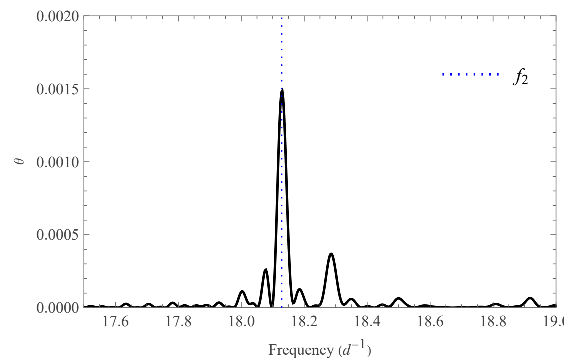

(d) The periodogram zoomed-in on f_2.

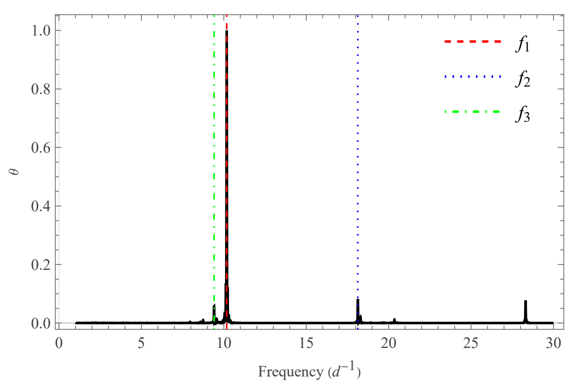

(e) The periodogram with f_1 prewhitened. There is still a large component of f_1 remaining, but f_3 is more distinctly visible.

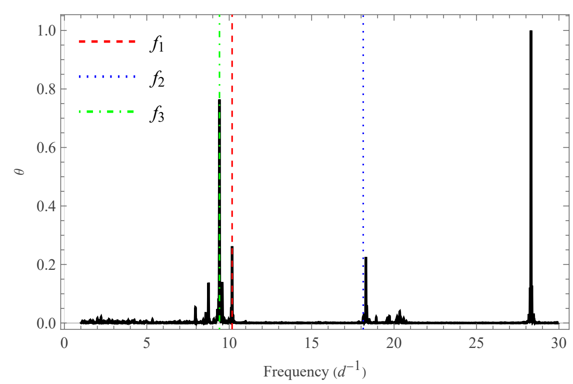

(f) The periodogram with f_1 prewhitened twice. Note that f_2 has a lower power than $f_1 + f_2$.

Figure 3.1 Frequency analysis of TESS observational data showing f_1, f_2, and f_3.

Table 3.1 High Frequencies found from Fourier analysis of TESS data.

	Frequency (c/d)	Power
f_1	10.1755	1
f_2	18.1282	0.001486
f_1+f_2	28.3072	0.001416
$2f_1$	20.3510	0.001147
f_3	9.4091	0.001042
$2f_1+f_2$	38.4811	0.00046

repeating artifact of removing f_1 (see figure 3.2a). More detailed analysis, which is beyond the scope of this thesis, is needed to confirm or reject f_3.

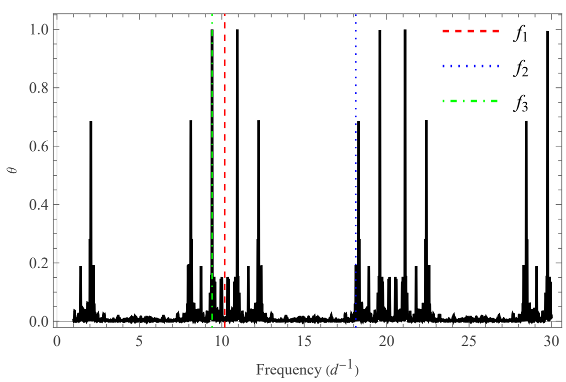

(a) The normalized Periodogram of the TESS $O-C$ data points.

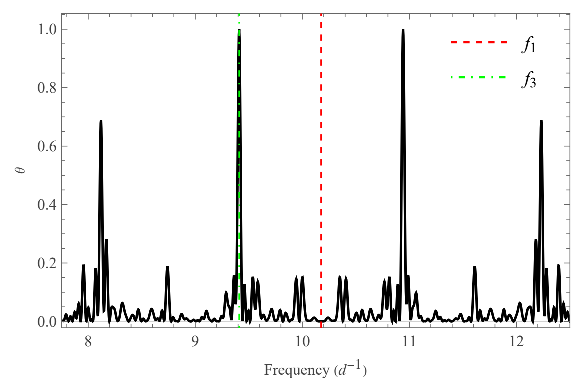

(b) A zoomed-in view of the $O-C$ periodogram.

Figure 3.2 The periodogram of TESS $O-C$ data. Note that running a Fourier analysis on $O-C$ data is functionally similar to removing f_1 from observational data. In this view, f_3 appears to be an artifact of removing f_1.

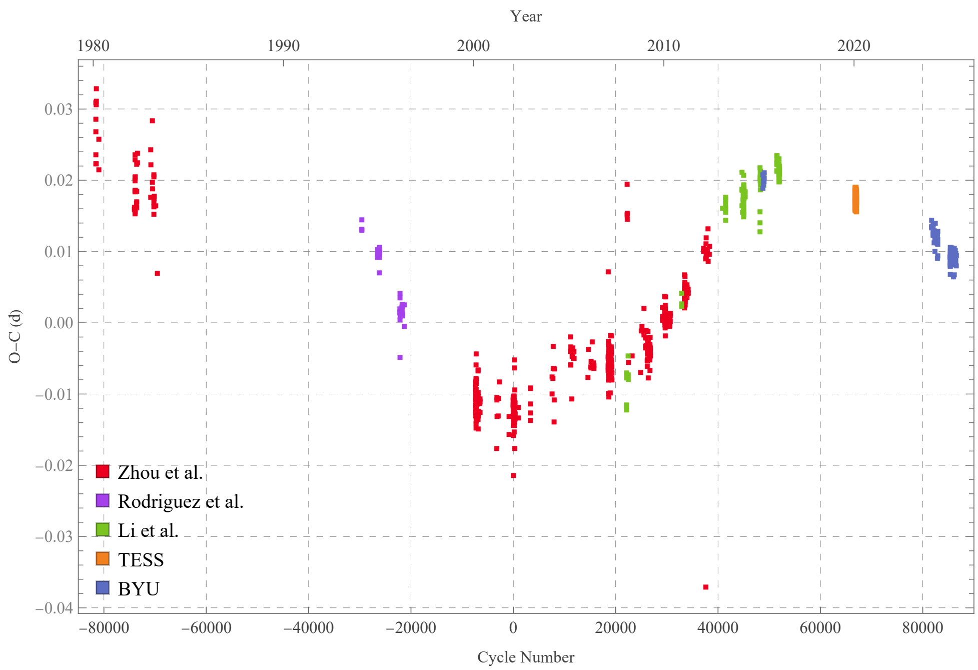

Figure 3.3 $O-C$ diagram using all collected maxima color-coded by source.

3.2 $O-C$ diagram

Using eq. 2.1, we created an $O-C$ diagram (figure 3.3). We then separated the $O-C$ values by observational season (roughly Dec-Apr) to determine outliers. First, potential outliers were selected by inspection. Next, we calculated the mean $O-C$ value and its standard deviation (excluding the previously selected potential outliers) from each season. We concluded that points lying more than three standard deviations away from this seasonal mean were outliers and did not include them in our analysis. The $O-C$ diagram which excludes outliers is in figure 3.4.

This $O-C$ diagram clearly shows a sinusoidal pattern which can be explained by the light-time travel effect (LTTE). The LTTE appears in stars that orbit around companions. It is the result of a maximum occurring earlier or later than expected (i.e. having an $O-C$ value higher or lower than 0) due to the difference in time required for the light to reach the observer from different positions in an orbit. Lower values result from maxima which occur when the star is closer to the observer

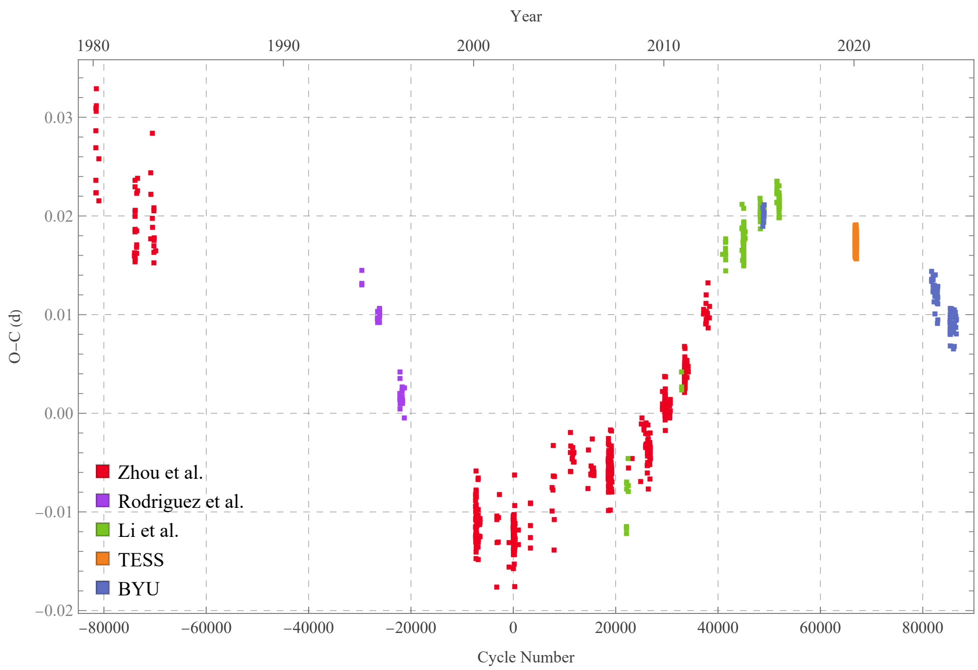

Figure 3.4 $O-C$ diagram with outliers removed.

while higher values result when the star is farther away. The radius of an orbit is related to the amplitude of an LTTE best-fit sine curve through the equation:

$$r = A_{LTTE} \times c$$

where r is the radius of the orbit in meters, A_{LTTE} is the amplitude of the LTTE best-fit sine in days, and c is the speed of light in meters/day (or alternatively: A_{LTTE} is converted to seconds and c is in meters/second). The period of the LTTE best-fit sine corresponds to the period of the orbit. We present the analysis of several models of 3-body LTTE fits later in this paper.

Although AN Lyn has been identified as a likely candidate for a 2- or 3-body system, its $O-C$ behavior has not been adequately studied due to the long period of the sinusoidal fit, differing ephemerides, and a lack of observational data (Hintz et al. 2005; Li et al. 2018; Zhou et al. 2017). The extended period in which we have observational data presented in this work, along with the

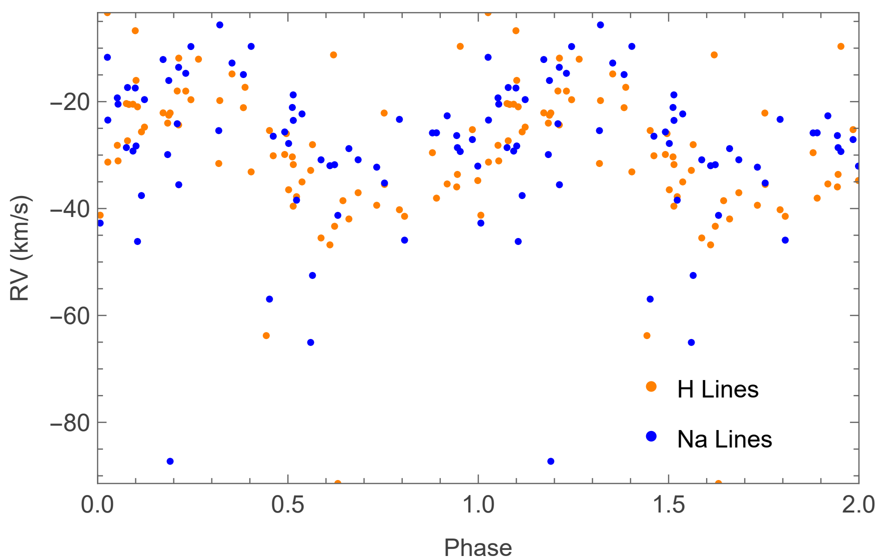

Figure 3.5 Phased AN Lyn radial velocity phase plot based on hydrogen lines (orange) and the sodium doublet (blue).

primary pulsation period derived from the TESS data, allows clearer and more certain analysis than has been achievable up to this point.

3.3 Radial Velocities

Using the RVs we derived from our spectral data, we calculated three different sets of redshifts for AN Lyn. First, we calculated redshifts in the the H and Na lines independently; next, we calculated redshifts in both H and Na lines together. We determined that both H and Na lines were features of AN Lyn's atmosphere. Because the Na lines showed more scatter and caused more scatter in the joint redshift calculations, we used the radial velocities calculated from the two H lines in our final analysis. Figure 3.5 shows the radial velocities calculated from H and Na phased by AN Lyn's primary pulsation period.

Radial velocities for 2004 and 2011 included consecutive spectra taken over the course of an entire pulsation period, while data from 2015-2021 contained only 2 observations per night. We separated our calculated redshifts by observational season and combined the six seasons without a full recorded cycle into three sets of data points (2015–2016, 2017–2018, and 2020–2021) to increase the number of data points available for fitting.

For each of our five seasons of spectra, we subtracted the zero point of our ephemeris and phased them by P_1 to account for movement due to pulsation. Next, we fit a sine wave to two phases of each set and collected average radial velocities, amplitudes of pulsation, and phase shifts. These parameters are recorded in table 3.2.

Table 3.2 Average radial velocity, amplitude, and measured phase shift by observing season.

Season	Average RV ($\mathrm{km\,s^{-1}}$)	Amplitude ($\mathrm{km\,s^{-1}}$)	Phase Shift
2005*	−36.5(0.5)	4.3(0.6)	0.32(2)
2011	−28.8(1.8)	18.8(2.5)	0.57(2)
2015–2016	−31.3(7)	12.9(1.2)	0.75(1)
2017–2018	−30.9(2.1)	10.4(3.1)	0.75(4)
2020–2021	−28.9(1.1)	12.6(1.7)	0.71(2)

*2005 data were taken from Hintz et al. (2005).

The phase shift is particularly relevant to our discussion because it reflects the LTTE seen in the $O-C$ diagram. This phase shift is produced when AN Lyn is farther from the Sun in its orbit, and we observe the spectra later. Therefore, there is a connection between phase shift and orbital location. We defined phase shift as the offset in phase from zero to the first RV maximum in the best-fit sine to the phased RV curve (we used the maximum because our phased data had more points around the maximum than minimum which provided a better fit). It has been shown that δ Scuti stars have a 0.090(15) phase shift between light curve maximum and RV minimum (Breger et al. 1976). AN Lyn's light curve is asymmetric (as is the RV curve), and the difference between

RV minimum and maximum is approximately 0.4 cycles. Therefore, in order to move from RV space to $O-C$ space, we subtracted $(0.4+0.09)$ from our phase shift and multiplied the result by P_1. The resultant $O-C$ values are contained in the last column of table 3.3 and are plotted in fig 3.6. As can be seen, these values agree well with photometric data.

Table 3.3 Corrected phase shifts and corresponding $O-C$ values by observing season.

Season	Phase Shift (corrected)	$O-C$
2005*	−0.169(35)	−0.017(34)
2011	0.083(35)	0.008(34)
2015–2016	0.263(25)	0.026(25)
2017–2018	0.257(55)	0.025(54)
2020–2021	0.217(35)	0.021(34)

*2005 data were taken from Hintz et al. (2005)

3.4 Long-term Periods

As evidenced by the LTTE in its $O-C$ diagram, AN Lyn has a companion star. After creating several models, we concluded that AN Lyn is well-modeled as having a third companion, as has been suggested (Li et al. 2018). We created a number of models to study AN Lyn and its companions. The construction of each model is summarized in table 3.5. For each model, we used a least-squares fit and, unless otherwise stated, gave equal weight to each observation. The orbital period and radius of AN Lyn's orbit with its outer companion (T_{out} and R_{out} respectively), the orbital period and radius of AN Lyn's orbit with its inner companion (T_{in} and R_{in} respectively), the root mean squared error (RMSE), and the skewness of residuals to model fits are collected in table 3.4. We present these

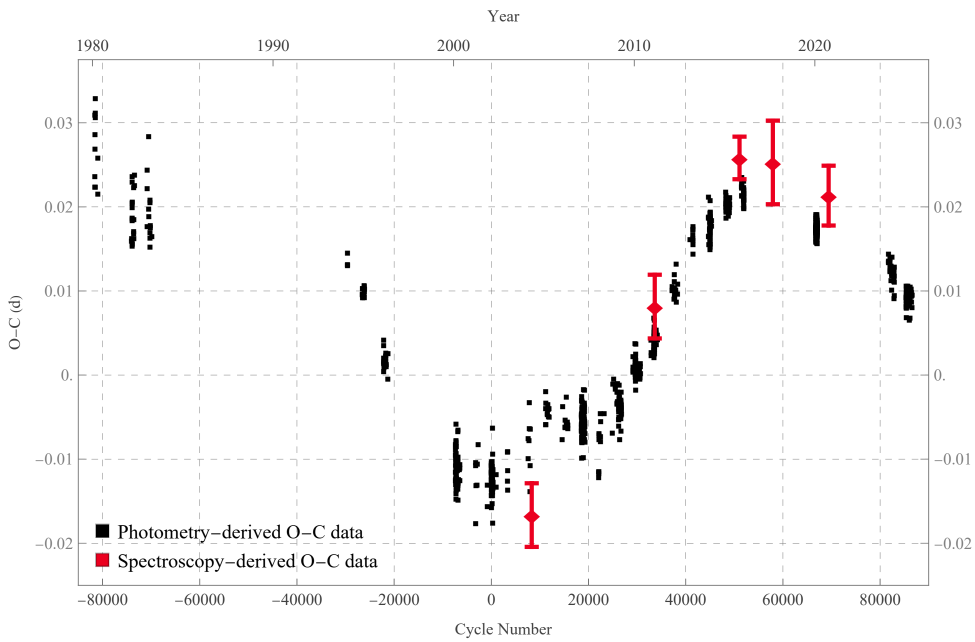

Figure 3.6 $O-C$ diagram including the $O-C$ values calculated from the phase shift in radial velocity measurements

models, the methods for creating them and relevant analysis in the following. In Chapter 4, we will discuss the strengths, weaknesses, and implications of the models.

Model 1

Model 1 is the simplest model but certainly not the best. Created from a single best-fit sine curve to our $O-C$ data, Model 1 implies a single companion. (see figure 3.7a). However, the plot of the residuals (fig 3.7b) shows a clear sinusoidal pattern indicating a secondary orbit and hence a three-body system. The clear pattern in the residuals (figure 3.7b) helps us rule out Model 1 as a compelling explanation of AN Lyn's LTTE.

Model 2

Model 2 was created by adding model 1 to the best-fit sine of its residuals. This model is the simplest extension of Model 1, assuming a constant pulsation period and two circular orbits. As

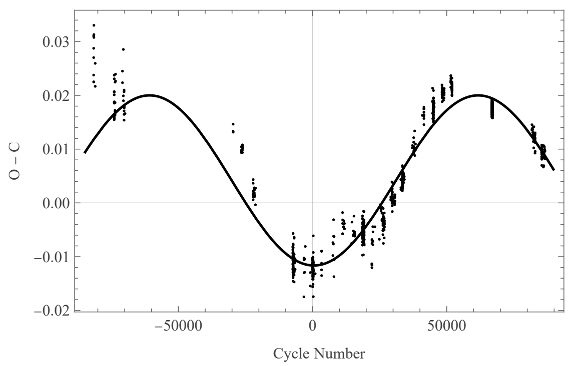

(a) Model 1 plotted over the $O-C$ diagram

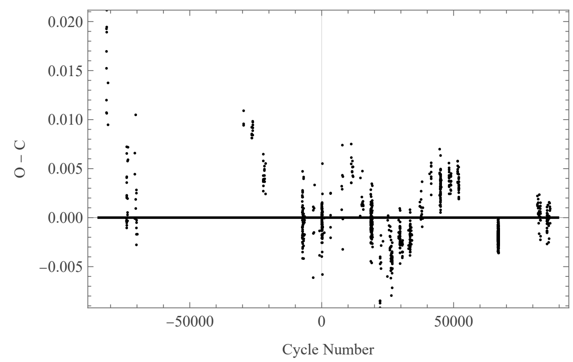

(b) Model 1 Residuals

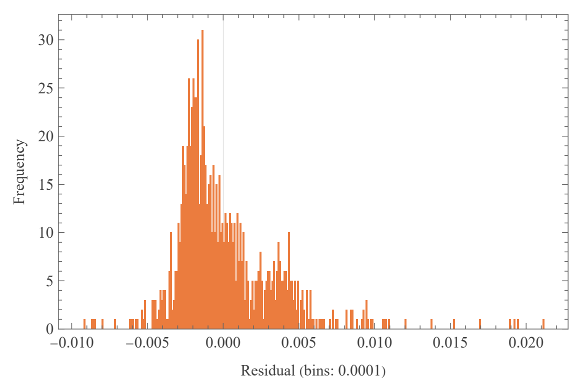

(c) Model 1 Histogram

Figure 3.7 Model 1. A single best-fit sine was applied to the $O-C$ data.

Table 3.4 Model Orbital Parameters and Statistics. Model 1 describes a single-orbit (two-body) system, while Models 2–8 describe double-orbit (three-body) systems. For a description of each model's construction, see Table 3.5.

Model	T_{out} (yr)	R_{out} (AU)	T_{in} (yr)	R_{in} (AU)	RMSE	Skewness
Model 1	32.94(20)	2.74(3)	-	-	0.00332	1.756
Model 2	32.94(20)	2.74(3)	11.53(7)	0.60(2)	0.00250	1.807
Model 3	30.37(15)	2.77(2)	9.65(7)	0.48(1)	0.00348	4.849
Model 4	32.94(20)	2.74(3)	11.89(8)	0.48(2)	0.00243	-0.266
Model 5	31.80(14)	2.84(2)	11.69(8)	0.50(2)	0.00222	0.120
Model 6	32.84(1.14)	2.74(16)	11.50(38)	0.59(13)	0.00418	1.524
Model 7	32.78(1.14)	2.73(10)	11.54(37)	0.60(13)	0.00406	1.537
Model 8	30.13	2.91(2)	9.98	0.39(2)	0.00259	3.818

seen in figure 3.8, Model 2 follows the data fairly well with the exception of the first observational season, the three seasons from Rodriguez et al., and the last season. Because later data used more sophisticated imaging instruments and light curve analysis software, we would expect the model to fit the newest data closely. Because it does not fit the most recent season, we conclude that this model may not tell the whole story.

Model 3

In order to prioritize more recent data, Model 3 (see figure 3.9) consists of a sine best-fit to $O-C$ data after 1990 (i.e., it was fit without the first three seasons). Model 3 follows most of the $O-C$ values used to calculate it—in particular, it remains close to the values calculated by Rodriguez et al. This is noteworthy as those three seasons are not well fit by most of the models. The early data are not fit well by this model, resulting in a high RMSE and the most extreme skew of any model. This is not enough to completely discount the model. The large gap in data between cycles -70,000

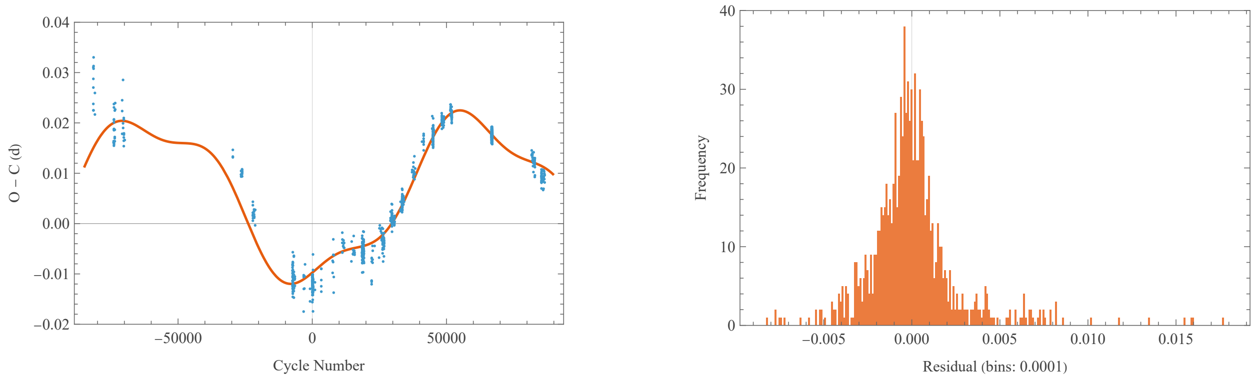

(a) Model 2 plotted over the $O-C$ diagram **(b)** Model 2 Histogram

Figure 3.8 Model 2. A best-fit sine was applied and subtracted from the $O-C$ data, then another sine was applied to the residuals.

and -30,000 leaves us guessing at what changes AN Lyn may have been undergoing. We note that the last season from Li et al. (2018) (just after 50,000 cycles) appears to deviate slightly from this model.

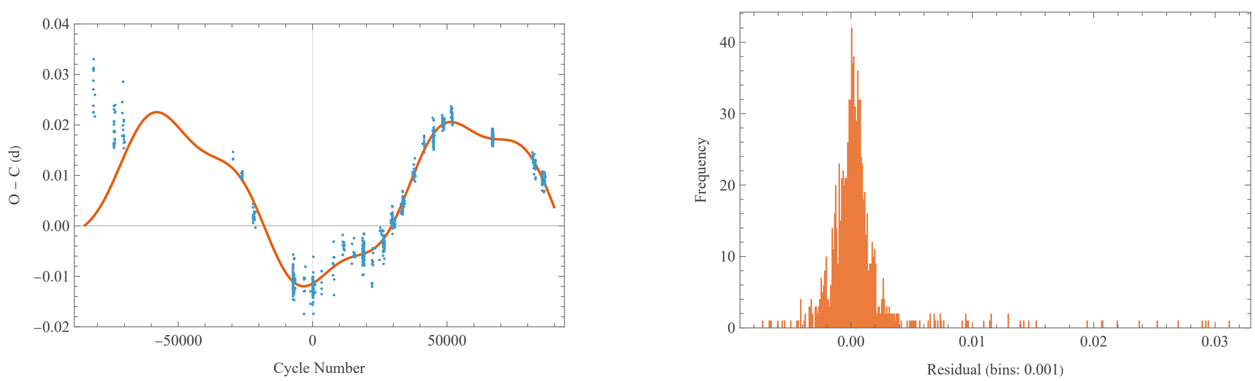

(a) Model 3 plotted over the $O-C$ diagram **(b)** Model 3 Histogram

Figure 3.9 Model 3. A best-fit sine was applied and subtracted from the $O-C$ data excluding data before 1990, then another sine was applied to the residuals.

Model 4

Many variable stars exhibit a constant period change. This can be modeled as

$$t_C = t_0 + P_0 E + \frac{1}{2}\frac{dP}{dt}\bar{P}E^2$$

or, equivalently, (**?**)

$$O - C = \frac{1}{2}\frac{dP}{dt}\bar{P}E^2,$$

where t_C and t_0 are the calculated time and the zero-point time respectively. Because our fitting software got stuck when fitting multiple sines and quadratics together, we applied best-fit curves one at a time. Since the dominant $O-C$ trend was a sinusoidal orbital effect, we first subtracted Model 1, then fit a quadratic to the residuals. After subtracting the quadratic, we fit a sine. The addition of the two sine curves and the quadratic constitutes Model 4 (see figure 3.10). From our fit, we found that $\frac{1}{2}\dot{P}\bar{P} = 4.00653810^{-13}$. Substituting P_0 for $\bar{P}$ (changes in period are negligible) and solving for $\dot{P}$, we find that $\frac{1}{P}\frac{dP}{dt} = 3.030410^{-8} yr^{-1}$. We note that despite its low RMSE and symmetric residual histogram, Model 4 under fits the maxima from Rodriguez et al. (1997a;b) and many of the maxima from 2010–2020.

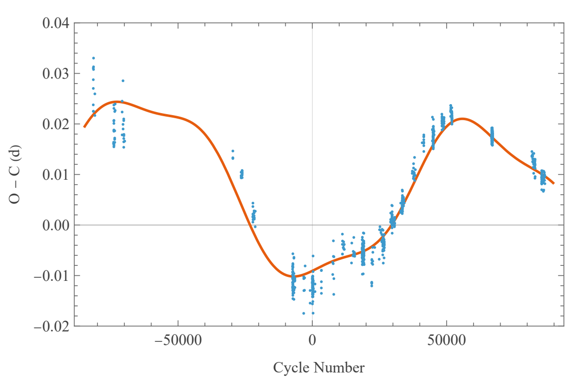

(a) Model 4 plotted over the $O-C$ diagram

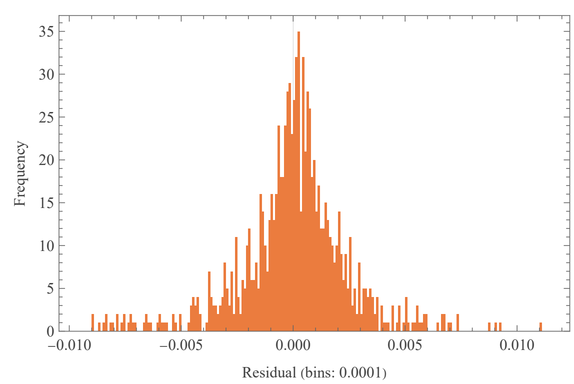

(b) Model 4 Histogram

Figure 3.10 Model 4. A best-fit sine, followed by a best-fit quadratic, was applied and subtracted from the $O-C$ data, then another sine was applied to the residuals.

Model 5

Model 5 (see figure 3.11) is similar to Model 4, but with the quadratic subtracted before any sine waves were fit. The obvious sinusoidal pattern in the $O-C$ makes an initial quadratic fit unreliable, so we used the same quadratic that was fit in Model 4. This improves the fit slightly and yields the lowest RMSE and most symmetric residuals.

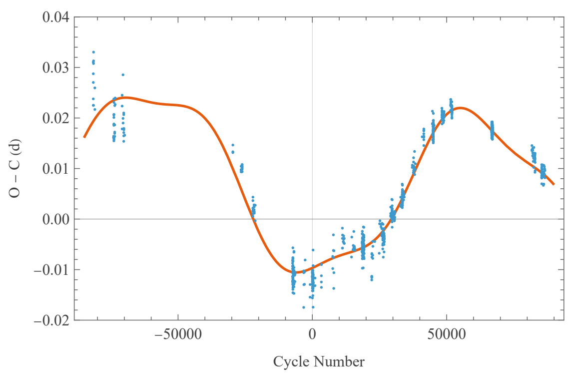

(a) Model 5 plotted over the $O-C$ diagram

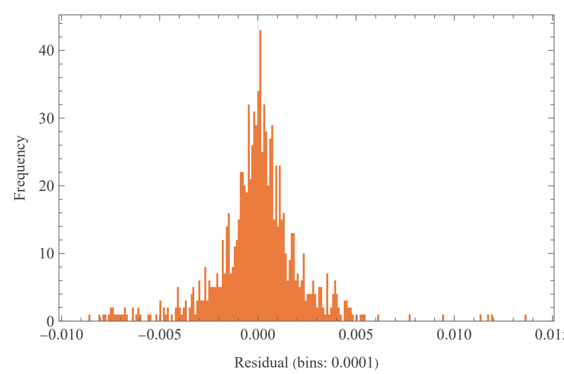

(b) Model 5 Histogram

Figure 3.11 Model 5. The best-fit quadratic from Model 4, followed by a best-fit sine, was subtracted from the $O-C$ data, then another sine was applied to the residuals.

Models 6 and 7

Models 6 and 7 (figures 3.12 and 3.13) were constructed by taking the mean and median $O-C$ value, respectively, and mean cycle number from each observational season and weighting it by the number of observations during that season. Both models fit newer data fairly well but diverge for early data sets. The RMSE and skewness values reported in table 3.4 were first calculated from the single-point seasons then multiplied by the season's weight.

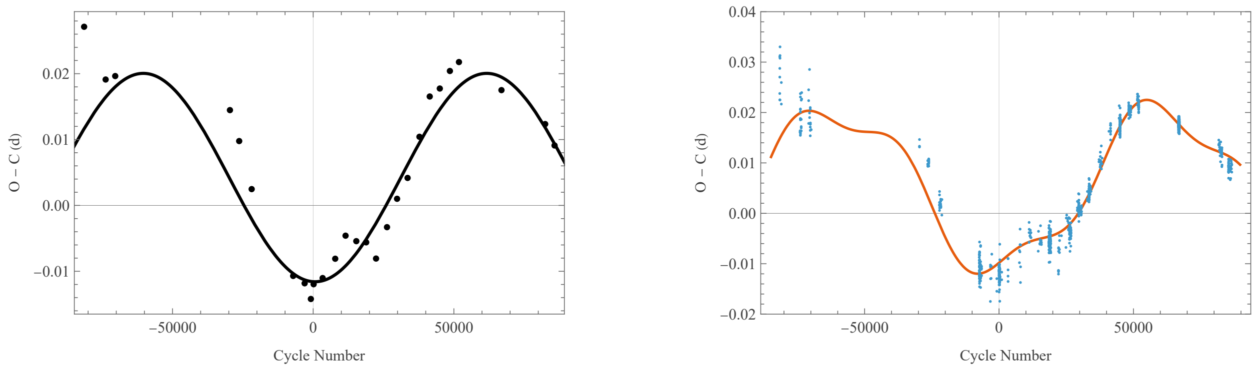

(a) Best fit line to the seasonal means **(b)** Model 6 plotted over the $O-C$ diagram

Figure 3.12 Model 6. A best-fit sine was applied and subtracted from the mean $O-C$ value from each observation season, then another sine was applied to the residuals.

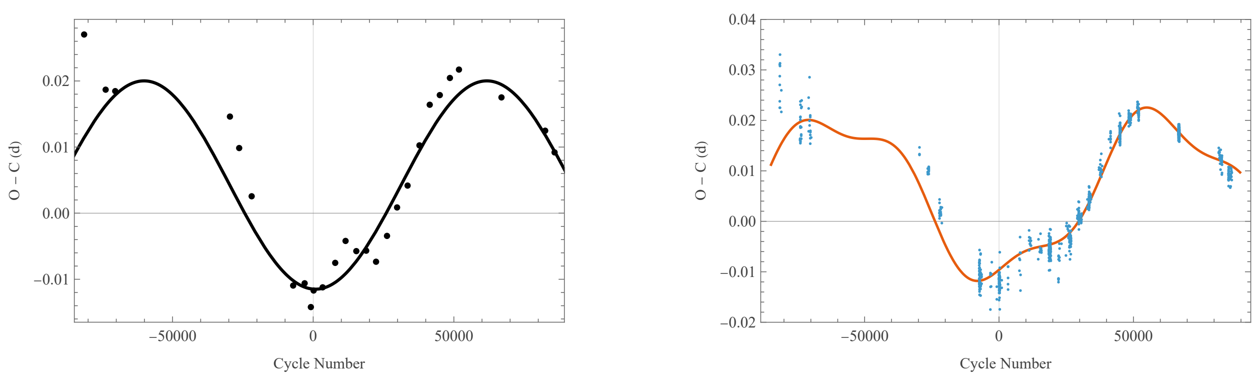

(a) Best fit line to the seasonal medians **(b)** Model 7 plotted over the $O-C$ diagram

Figure 3.13 Model 7. A best-fit sine was applied and subtracted from the median $O-C$ value from each observation season, then another sine was applied to the residuals.

Model 8

Model 8 is our final model (see figure 3.14). We constructed it by subtracting the quadratic from Model 4 and then manually testing sine waves with different periods and choosing those that appeared to fit our data best. To make this easier, we phase-folded our $O-C$ data and searched for the best period. With the exception of the very first observational season, this model shows very good agreement with the $O-C$ data. Notably, it stays very close to the Rodriguez et al. data while still keeping with newer data. Despite the low RMSE, the first season is not fit well, causing the extreme skew in Model 8.

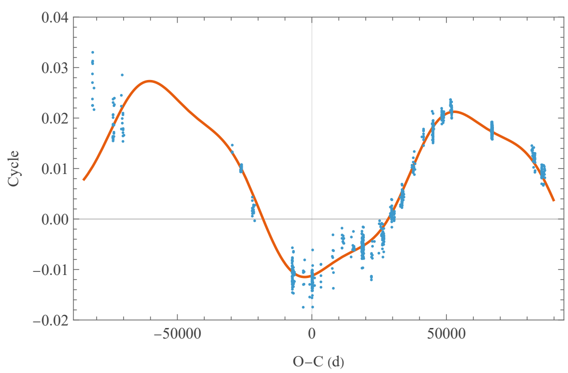

(a) Model 8 plotted over the $O-C$ diagram

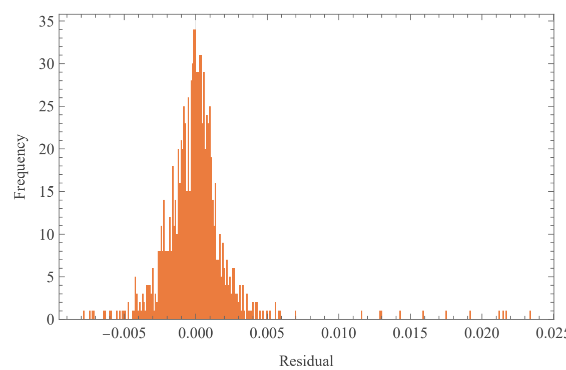

(b) Model 8 Histogram

Figure 3.14 Model 8. The quadratic from Model 4 was subtracted. Then, a sine was fit by manually identifying the best-looking period to phase-fold the $O-C$ data, then a second sine was applied via the same method to the residuals.

Table 3.5 Summary of models applied to the $O-C$ data.

Name	Description
Model 1	A single best-fit sine was applied to the $O-C$ data.
Model 2	A best-fit sine was applied and subtracted from the $O-C$ data, then another sine was applied to the residuals.
Model 3	A best-fit sine was applied and subtracted from the $O-C$ data excluding data before 1990, then another sine was applied to the residuals.
Model 4	A best-fit sine, followed by a best-fit quadratic, was applied and subtracted from the $O-C$ data, then another sine was applied to the residuals.
Model 5	The best-fit quadratic from Model 4, followed by a best-fit sine, was subtracted from the $O-C$ data, then another sine was applied to the residuals.
Model 6	A best-fit sine was applied and subtracted from the mean $O-C$ value from each observation season, then another sine was applied to the residuals.
Model 7	A best-fit sine was applied and subtracted from the median $O-C$ value from each observation season, then another sine was applied to the residuals.
Model 8	The quadratic from Model 4 was subtracted. Then, a sine was fit by manually identifying the best-looking period to phase-fold the $O-C$ data, then a second sine was applied via the same method to the residuals.

Chapter 4

Discussion and Conclusions

In this study, we attempted to explain AN Lyn's $O-C$ behvior. We analyzed 319 new maxima for the δ Scuti star AN Lyn. Due to the lack of atmospheric effects and the long-term continuity, data taken from NASA's TESS are the highest quality photometric observations we have of AN Lyn to date. Thus, these data were used to determine a precise primary pulsation frequency, f_1, corresponding to $P_1 = 0.09827475(49)$. We used f_1 to determine a new ephemeris (see equation 2.1) and improve on previously published $O-C$ diagrams. We also found f_3, a frequency that was previously found in one study but not in others (Rodriguez et al. 1997a). Finally, we constructed 8 orbital models using different lines of best fit to the $O-C$ diagram and concluded that AN Lyn is well-modeled as a three-body system. The orbital parameters obtained from the fits of each model are contained in table 3.4.

4.1 Analysis of models

Upon visual inspection of these 8 models and their residuals, we can discard several as bad fits to the data. Model 1 is an important fit since many other models build off of it, but the clear pattern in the residuals indicates it does not capture the behavior of AN Lyn's $O-C$ diagram. Models 6 and 7 were approximations, so they were not expected to be the most accurate. However, they make good reference points for the general behavior of our models. Notably, they fit more recent data closely but miss the first season as well as the seasons between cycles $-40,000$ and $-20,000$. We see that this is a reoccurring problem with several models which may be due to lower precision in older data compared to newer data.

Next, we address the best models according to the RMSE. Model 5 has the lowest RMSE followed by Model 4 since they fit the early data well. However, upon closer inspection of these two models, we see that neither fits the data between 30,000 and 50,000. This is a problem because these data are more precise than the earlier seasons. Model 2 also has a low RMSE, but for a different reason: it is a relatively good fit to the recent data. However, Model 2 under-predicts the first observational season, raising its RMSE above models 4 and 5.

As improved technology is integrated into observations, precision in light detection and time recording improves. This was the motivation for Model 3. Due to the method of constructing Model 3, it fits recent data well but misses the first 3 seasons altogether. This results in a high RMSE and extreme skew in the residuals. In general, skewness is not an adequate measure of model fidelity because it does not take into account the precision/uncertainty of the data. As such, the skewness of Model 3 is not enough to disqualify it. Similarly, Model 8 has low RMSE and high skewness. One strength of models 3 and 8 over all other models is how well they fit data between cycle numbers -40,000 and -20,000. It is interesting to note that these two models have the shortest T_{out}.

As of now, there is no one model which appears strictly better than all others. Future observations will help confirm (and constrain) them. We submit that the most promising models are 2, 3, and 8 because they predict data since 2010 the best. Since there was no clear best model, we derived orbital parameters from each model (see table 3.4). We find that AN Lyn is best modeled as a 3-body system with orbital parameters lying somewhere within the ranges listed in table 4.1.

Table 4.1 Orbital parameters of AN Lyn and its companions.

T_{out} (yr)	R_{out} (AU)	T_{in} (yr)	R_{in} (AU)
30.13–32.94	2.72–2.93	9.58–11.97	0.37–0.61

Using these parameters and AN Lyn's mass, we can solve for minimum masses ($M\sin i$) in the AN Lyn system. Li et al. (2018) found the mass of AN Lyn to be $1.70 \pm 0.05 M_{\odot}$. Using this mass, a lower threshold can be calculated for the masses of AN Lyn's companions using Kepler's third law in solar units:

$$a_{\rm in}^3 = (M_{AN} + M_{in})\, T_{\rm in}^2, \tag{4.1}$$

where a_{in} is the separation between AN Lyn and its inner companion and M_{in} is the minimum mass of its inner companion. Letting R_{in} be the observed orbital radius of AN Lyn, we also find

$$\frac{a_{\rm in}}{R_{\rm in}} = \frac{M_{AN} + M_{in}}{M_{in}} \quad \Rightarrow \quad a_{\rm in} = R_{\rm in} \frac{M_{AN} + M_{in}}{M_{in}}. \tag{4.2}$$

Substituting into Kepler's law gives

$$R_{\rm in}^3 \frac{(M_{AN} + M_{in})^3}{M_{in}^3} = (M_{AN} + M_{in})\, T_{\rm in}^2. \tag{4.3}$$

Rearranging, we obtain

$$\frac{M_{in}^3}{(M_{AN} + M_{in})^2} = \frac{R_{\rm in}^3}{T_{\rm in}^2}. \tag{4.4}$$

Similarly, we find

$$\frac{M_{out}^3}{(M_{AN} + M_{in} + M_{out})^2} = \frac{R_{\rm out}^3}{T_{\rm out}^2}, \tag{4.5}$$

where M_{out} is the minimum mass of AN Lyn's outer companion.

Solving these equations numerically for M_{in} and M_{out} gives lower bounds on the masses of AN Lyn's companions. Since we have multiple different models, we performed a Monte Carlo simulation varying orbital parameters within their measured uncertainties to estimate the masses of AN Lyn's inner and outer companions. The simulation yields median masses of

$$M_{in} = 0.1535^{+0.0300}_{-0.0221}\, M_{\odot} \quad \text{and} \quad M_{out} = 0.4896^{+0.0293}_{-0.0277}\, M_{\odot}.$$

Table 4.2 Approximate stellar parameters of AN Lyn's companions based on the minimum mass calculated ($m \sin i$).

Companion	Minimum Mass ($M_\odot$)	Spectral Type	Luminosity ($L_\odot$)	Radius ($R_\odot$)	T_e (K)
Inner	0.1535	M5	0.0076	0.29	3170
Outer	0.4896	M1	0.050	0.56	3660

Based on these minimum masses, we can find approximate minimum values for luminosity, radius, and effective temperature based on the spectral type. These values are summarized in table 4.2. The approximate spectral types, luminosities, radii, and effective temperatures were taken from Appendix G of Carroll & Ostlie (2017).

These masses and their respective luminosities are supported by the fact that there are no spectral line contributions from either companion. Therefore, the luminosity of the system must be dominated by AN Lyn. The mass of the outer companion is in good agreement with the findings of Li et al. (2018); however, we found the mass of the inner companion to be only half of what they suggested.

4.2 Future Work

Future observations could determine which of the proposed models most accurately predicts AN Lyn's behavior or if a new model is needed. Further analysis of AN Lyn's pulsation periods is necessary to confirm or reject f_3 as an independent frequency. In addition, more spectra over an entire pulsation period would better constrain AN Lyn's pulsation and orbital properties. Further analysis of the stability of the system given these minimum mass parameters could also strengthen or challenge the three-body LTTE as the explanation of AN Lyn's $O-C$ curve. This might include a comparison between AN Lyn and other known 3-body systems. In summary, AN Lyn is an intriguing target as a 3-body system with a δ Scuti primary.

Appendix A

Tables of Maxima

Table A.1 63 maxima obtained from the OPO. Times are in HJD.

2460339.8722908	2460340.8548782	2460340.9541561
2460368.8622254	2460368.9610173	2460369.8448615
2460369.8460401	2460369.9446794	2460388.8108354
2460390.7780118	2460403.7491867	2460403.7493821
2460403.7502016	2460404.7301611	2460404.8307252
2460411.7115976	2460445.7118222	2460445.7126540
2460446.6948863	2460446.6957254	2460447.6781326
2460447.6781695	2460452.6872662	2460452.6907106
2460457.7019149	2460457.7030251	2460458.6823448
2460458.6839726	2460692.9691129	2460696.9976414
2460696.9985700	2460697.9800899	2460697.9808132
2460697.9825237	2460698.9644101	2460698.9646432
2460699.7488295	2460699.7489078	2460699.8459651

Continued on next page

Table A.1 – *Continued from previous page*

2460699.9455634	2460703.9755457	2460703.9758741
2460703.9768959	2460716.6530450	2460719.7003573
2460729.6255135	2460729.7252273	2460733.6546239
2460745.6443447	2460759.6949798	2460759.7951621
2460759.8939163	2460761.8587049	2460775.7140156
2460775.8145771	2460776.7987408	2460776.8955826
2460796.7482680	2460803.7242288	2460804.7080986
2460805.6904420	2460815.7130925	2460817.6800571

Table A.2 9 maxima obtained from the WMO. Times are in HJD.

2457101.6265336	2457101.7267022	2457108.7032868
2457108.8010396	2457116.7622065	2457116.8604242
2457123.7393313	2457126.6880062	2457126.787056

Table A.3 247 maxima obtained from TESS observations. Times are in HJD.

2458870.5695259	2458870.6681951	2458870.7668628
2458870.8653403	2458870.9636713	2458871.0629948
2458871.1615048	2458871.2600050	2458871.3564739
2458871.4546205	2458871.5532497	2458871.6518650
2458871.7496638	2458871.8465259	2458871.9447070
2458872.0443353	2458872.1430592	2458872.2412057
2458872.3389607	2458872.4374372	2458872.5367944
2458872.6353191	2458872.7325091	2458872.8303042

Continued on next page

Table A.3 – *Continued from previous page*

2458872.9282085	2458873.0272976	2458873.1258083
2458873.2235771	2458873.3209760	2458873.4193141
2458873.5182075	2458873.6167838	2458873.7151627
2458873.8137567	2458873.9121541	2458874.0105916
2458874.1082759	2458874.2066754	2458874.3035661
2458874.4023995	2458874.5013244	2458874.6004466
2458874.6984966	2458874.7960872	2458874.8943567
2458874.9930014	2458875.0918278	2458875.1903569
2458875.2878361	2458875.3854369	2458875.4836838
2458875.5819811	2458875.6811247	2458875.7786448
2458875.8770329	2458875.9753968	2458876.0740397
2458876.1722573	2458876.2700931	2458876.3689665
2458876.4668207	2458876.5662000	2458876.6644082
2458876.7619401	2458876.8594030	2458876.9583625
2458877.0566419	2458877.1543386	2458877.2529224
2458877.3509905	2458877.4496643	2458877.5478311
2458877.6455666	2458877.7445210	2458877.8422300
2458877.9415024	2458878.0398033	2458878.1371075
2458878.2342632	2458878.3333060	2458878.4321330
2458878.5303103	2458878.6278370	2458878.7263264
2458878.8251065	2458878.9240103	2458879.0216940
2458879.1198851	2458879.2186780	2458879.3173804
2458879.4156685	2458879.5136904	2458879.6114782

Continued on next page

Table A.3 – *Continued from previous page*

2458879.7093314	2458879.8077983	2458879.9064732
2458880.0045097	2458880.1031180	2458880.2018271
2458880.2999245	2458880.3985165	2458880.4963834
2458880.5948358	2458880.6929726	2458880.7909586
2458880.8889278	2458880.9871737	2458881.0849749
2458881.1836707	2458881.2823958	2458881.3806575
2458881.4792623	2458881.5781403	2458881.6760115
2458881.7743742	2458881.8719326	2458881.9701174
2458882.0688676	2458882.1664856	2458882.2651045
2458882.3625599	2458882.4610882	2458882.5589284
2458882.6573469	2458882.7561886	2458882.8553155
2458882.9533363	2458883.0512198	2458883.1494638
2458883.2478386	2458883.3466006	2458883.4446784
2458883.5423707	2458883.6404132	2458883.7388072
2458883.8375018	2458883.9358163	2458886.9828704
2458887.0817970	2458887.1796277	2458887.2770871
2458887.3751646	2458887.4726612	2458887.5713848
2458887.6703701	2458887.7687397	2458887.8664150
2458887.9648774	2458888.0637469	2458888.1630899
2458888.2604006	2458888.3591267	2458888.4571122
2458888.5554049	2458888.6535561	2458888.7510186
2458888.8480601	2458888.9460734	2458889.0452216
2458889.1447379	2458889.2432625	2458889.3408003

Continued on next page

Table A.3 – *Continued from previous page*

2458889.4387832	2458889.5379111	2458889.6363312
2458889.7356800	2458889.8327769	2458889.9299307
2458890.0279443	2458890.1272697	2458890.2247857
2458890.3225913	2458890.4205978	2458890.5196885
2458890.6187238	2458890.7165595	2458890.8142930
2458890.9128962	2458891.0116006	2458891.1097329
2458891.2076936	2458891.3048205	2458891.4035893
2458891.5028604	2458891.6011879	2458891.6997549
2458891.7969891	2458891.8958826	2458891.9952843
2458892.0939622	2458892.1915032	2458892.2887454
2458892.3869918	2458892.4858353	2458892.5849607
2458892.6822248	2458892.7798956	2458892.8782470
2458892.9775191	2458893.0759795	2458893.1743617
2458893.2723340	2458893.3707549	2458893.4694240
2458893.5672903	2458893.6653563	2458893.7623380
2458893.8608182	2458893.9590030	2458894.0578415
2458894.1564115	2458894.2534116	2458894.3518923
2458894.4510666	2458894.5500647	2458894.6489435
2458894.7468288	2458894.8442725	2458894.9430556
2458895.0414274	2458895.1390359	2458895.2356694
2458895.3343896	2458895.4334573	2458895.5325763
2458895.6298051	2458895.7278523	2458895.8262432
2458895.9254983	2458896.0246069	2458896.1225774

Continued on next page

Table A.3 – *Continued from previous page*

2458896.2201151	2458896.3178666	2458896.4171315
2458896.5150265	2458896.6125537	2458896.7097422
2458896.8099449	2458896.9083930	2458897.0064933
2458897.1041665	2458897.2026578	2458897.3018429
2458897.4004322	2458897.4981164	2458897.5956414
2458897.6939486		

Table A.4 35 maxima obtained from observations reported in Rodriguez et al. (1997a;b). Times are in HJD.

2449398.7479007	2449398.8460235	2449398.9457848
2449701.0374085	2449702.0202458	2449703.0036655
2449704.9680417	2449705.9508007	2449706.9338876
2449707.0328923	2449736.5121080	2449737.4001601
2449737.4974769	2449739.4625066	2449740.5448386
2449741.5270003	2449742.4117580	2450130.3916220
2450130.4905104	2450131.3733949	2450131.4727834
2450131.5730235	2450132.4492055	2450132.5564527
2450136.3859058	2450136.4848562	2450143.4621818
2450172.7488496	2450174.7147821	2450174.8127406
2450175.7948390	2450181.7889246	2450183.7546914
2450216.3801268	2450219.4297267	

Bibliography

Agerer, F., Fernandes, M., & Frank, P. 1983, Information Bulletin on Variable Stars, 2370, 1, aDS Bibcode: 1983IBVS.2370....1A

Breger, M. 1979, Publications of the Astronomical Society of the Pacific, 91, 5

Breger, M., Hutchins, J., & Kuhi, L. V. 1976, The Astrophysical Journal, 210, 163, publisher: IOP ADS Bibcode: 1976ApJ...210..163B

Carroll, B. W., & Ostlie, D. A. 2017, An Introduction to Modern Astrophysics (Cambridge University Press), google-Books-ID: PY0wDwAAQBAJ

Collins, K. A., Kielkopf, J. F., Stassun, K. G., & Hessman, F. V. 2017, The Astronomical Journal, 153, 77

Handler, G. 2009, AIP Conference Proceedings, 1170, 403

Hintz, E. G., Bush, T. C., & Rose, M. B. 2005, The Astronomical Journal, 130, 2876, publisher: IOP Publishing

Li, G., Fu, J., Su, J., Fox-Machado, L., Michel, R., Guo, Z., Liu, J., & Feng, G. 2018, Monthly Notices of the Royal Astronomical Society, 473, 398

Paunzen, E., & Vanmunster, T. 2016, Astronomische Nachrichten, 337, 239, _eprint: https://onlinelibrary.wiley.com/doi/pdf/10.1002/asna.201512254

Percy, J. R. 2007, Understanding Variable Stars (Cambridge, UK: Cambridge University Press)

Ricker, G. R., et al. 2014, Journal of Astronomical Telescopes, Instruments, and Systems, 1, 014003

Rodriguez, E., Gonzalez-Bedolla, S. F., Rolland, A., Costa, V., & Lopez de Coca, P. 1997a, Astronomy and Astrophysics, 324, 959, aDS Bibcode: 1997A&A...324..959R

Rodriguez, E., Gonzalez-Bedolla, S. F., Rolland, A., Costa, V., Lopez-Gonzalez, M. J., & Lopez de Coca, P. 1997b, Astronomy and Astrophysics, 328, 235, aDS Bibcode: 1997A&A...328..235R

Sterken, C. 2005, in , 3, aDS Bibcode: 2005ASPC..335....3S

Yamasaki, A., Okazaki, A., & Kitamura, M. 1981, Publications of the Astronomical Society of the Pacific, 93, 77, publisher: IOP Publishing

Zhevakin, S. A. 1963, Annual Review of Astronomy and Astrophysics, 1, 367

Zhou, A.-Y. 2002, Astronomy & Astrophysics, 385, 503, number: 2 Publisher: EDP Sciences

Zhou, A.-Y., et al. 2017, A Pulsational Time-evolution Study for the δ Scuti Star AN Lyncis, arXiv:1710.03944 [astro-ph]

Index